ELSEVIER

Catalysis Today 53 (1999) 273–288

CATALYSIS TODAY

www.elsevier.com/locate/cattod

Simulations of the kinetics of rapid reactions on supported catalyst particles

H. Persson [a,*], P. Thormählen [a], V.P. Zhdanov [a,b], B. Kasemo [a]

[a] *Competence Centre for Catalysis and Department of Applied Physics, Chalmers University of Technology, SE-412 96, Göteborg, Sweden*
[b] *Boreskov Institute of Catalysis, Russian Academy of Sciences, Novosibirsk 630090, Russia*

Abstract

Recent simulations of the kinetics of heterogeneous reactions occurring on supported catalyst particles are briefly reviewed. The attention is focused on such effects inherent for nanometer chemistry as reactant supply via the support, interplay of the reaction kinetics on different facets, and adsorbate-induced reshaping of catalyst particles. In addition, original Monte-Carlo simulations are presented illustrating the contribution of the facet edges to the reaction rate. ©1999 Elsevier Science B.V. All rights reserved.

Keywords: Monte-Carlo simulations; Models of non-equilibrium phenomena; Models of surface chemical reactions; Catalysis

1. Introduction

Supported catalysts consist of small, typically 1–100 nm, particles of the active catalytic material, dispersed on and supported by a less active or totally inactive support [1]. The latter has a high porosity and thereby a large surface area (1–100 m^2/g or even larger). A typical example is the noble metal (Pt, Rh, and Pd) catalyst particles supported on alumina in three way catalytic converters of car exhaust gas [2]. A primary reason for this design of the catalyst is to achieve a high utilization of the catalytic material, through a high fraction of surface atoms. There are, however, other more subtle reasons, such as dependence of activity and selectivity, and maybe resistance to poisoning, on particle size.

A practical working catalyst commonly has a distribution of particle sizes and shapes, with domination of the (111) and (100) facets. From basic research on single crystals of catalytic materials, it is today well established that the rate of a catalytic reaction may vary considerably from one crystal face to another [3] and that defect sites such as steps, kinks, surface vacancies, adatoms etc., may have different catalytic activities than the perfect terrace sites [4]. In addition, there are (for supported catalysts) additional types of sites at the particle-support boundary. It is therefore not surprising that a wide variety of behaviour of catalytic activity versus particle size has been observed [5], sometimes differing considerably from single crystals. The collective set of such differences and the challenge to understand and explain them is referred to as the ‘structure gap’ in catalysis (sometimes also called the ‘materials gap’). Another way of expressing the structure gap is: to what extent are the single crystal data for catalytic kinetics representative of the catalytic kinetics measured for supported catalysts. (An

* Corresponding author. Tel.: +46-31-772-2967; fax: +46-31-772-3134
E-mail address: hans.persson@fy.chalmers.se (H. Persson)

0920-5861/99/$ – see front matter
PII: S0920-5861(99)00121-2

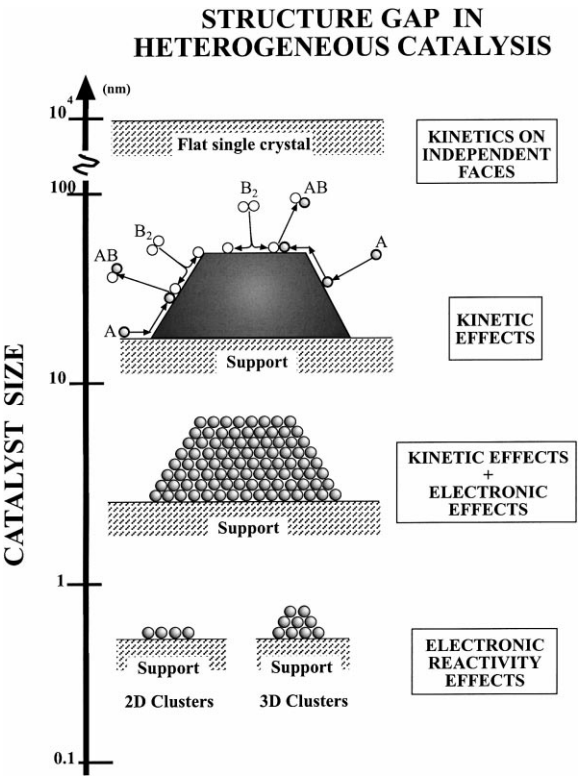

Fig. 1. Electronic and kinetic effects as an ingredient of the structure gap in heterogeneous catalysis.

additional complicating factor, not addressed here, is the so called 'pressure gap', expressing that practical conditions involve pressures of 1 atm or higher, while many of the most detailed studies have been performed at vacuum conditions, typically at 10^{-9}–10^{-4} Torr).

The question we are addressing in this paper is the structure gap (Fig. 1) or, more correctly, one particular aspect of the structure gap, since the latter has several components of quite different origins. At the smallest length scales of the order of 1 nm, metal particles have 2D or 3D sizes comparable to the electronic screening length in metals, and the electron structure is then significantly different from that of bulk metals. Consequently their catalytic activities are also different. At somewhat larger sizes, 3–4 nm, the electronic properties of the particles are already very close to that of the bulk metal, except at the atoms contacting or very near the support where so called (strong) metal support interaction (SMSI) [6] may modify the catalytic properties. The latter may be significantly perturbed, electronically, and thereby also have different catalytic activities. Since the particles are small, these sites may be important or even dominant for the overall catalytic kinetics. At even larger sizes, above about 10 nm, the particles are electronically essentially identical to bulk metals but may still exhibit remarkably different kinetics, compared to single crystals as shown below.

The topic of this article is to demonstrate these differences by simulations of the catalytic kinetics on particles large enough to have attained bulk electronic properties and ignoring SMSI effects. The basic underlying mechanisms for the phenomena – we describe and which do not occur on single crystals – are: (i) the different catalytic activities on different facets of a small supported crystalline particle become coupled in a strongly non-linear fashion due to diffusion occurring over facet boundaries, (ii) equilibrium-shape changes of small particles, caused by adsorbates, induce changes in catalytic behaviour, (iii) different kinetic rate constants at the facet boundaries of a supported particle compared to those for the perfect facets give rise to new kinetics, and (iv) spillover by diffusion of reactants, between the particle and its support, also create new kinetics. The subjects (i), (ii) and (iv), treated in our recent publications [7–10], are briefly discussed in Section 2 (a comprehensive review is submitted elsewhere [11]). Section 3 contains original results illustrating the effect of edges on the reaction kinetics on nm particles. As a generic example, we analyze in both sections a rapid *bistable* reaction with participation of simple molecules. (Simulations of catalytic reactions involving more complex molecules (long hydrocarbon chains) have recently been executed by McLeod and Gladden [12,13]. The latter works were focused on relating the reaction selectivity to the geometry of supported catalyst particles.)

The practical implications of the obtained results and the experimental possibilities to study the predicted effects are addressed in Section 4. It should be noted already here, however, that there has recently been a rapid development of techniques aimed at preparation of well controlled arrays of supported particles on planar surfaces, that mimic supported catalysts. For very small particles, these methods are, e.g., carefully controlled evaporation and annealing of condensed particles, or deposition of clusters by

cluster beams. The deposits are characterized by scanning probe techniques or electron microscopy. Such model systems were recently reviewed comprehensively by Henry [14]. For somewhat larger particles, electron beam lithography can be employed (so far for particles $\geq$10 nm) [6,15], to make nearly perfect arrays of supported particles. These experimental preparation techniques have demonstrated that it is possible to prepare particle arrays of fairly uniform size and shape distributions, which can be varied systematically. This motivates parallel simulations of the kinetics of such particles. We expect that the interplay between catalytic measurements on such particle arrays and corresponding simulations will rapidly improve our understanding of the catalytic kinetics on supported particles, and ultimately help to improve the design and function of practical supported catalysts.

2. Overview of earlier simulations

2.1. Model reaction

As an example, we treated in our studies [7–10] one of the generic catalytic reactions,

$$2A + B_2 \rightarrow 2AB, \tag{1}$$

occurring via the Langmuir–Hinshelwood (LH) mechanism,

$$A_{gas} \rightleftharpoons A_{ads}, \tag{2}$$

$$(B_2)_{gas} \rightarrow 2B_{ads}, \tag{3}$$

$$A_{ads} + B_{ads} \rightarrow (AB)_{gas}. \tag{4}$$

This reaction mimics, e.g., CO or hydrogen oxidation on noble metals (A stands for CO or hydrogen, and B_2 for O_2). During the past decade, its kinetics for the infinite surface have been studied in detail in the framework of the mean-field (MF) approximation (where surface diffusion of both reactants is implicitly assumed to be rapid compared to the LH step) and also by using Monte-Carlo (MC) simulations in the case of limited mobility of the reactants (see the reviews [16,17]). In our studies, we have used the MF kinetic equations (see e.g. Section 2.2) were appropriate, but the bulk of our results where obtained by employing the MC technique (this technique is necessary for a detailed analysis of rapid reactions at the nm scale).

MC simulations are far from straightforward if one wants to understand situations corresponding to real reactions, because in this case the ratio of the rate constants of different steps varies over many orders of magnitude. We paid special attention to this aspect of the reaction kinetics. In particular, we have focused on one of the most interesting situations (for justification, see [7]) namely when the LH step is fast compared to A and B_2 adsorption, B particles are (relatively) immobile, and A diffusion is rapid compared to the LH step. Although our main interest and dominating focus in this article are effects resulting from reactant diffusion between different facets of a single catalyst particle, we begin with the case of spillover between the support and a particle on the support.

2.2. Reactant supply via the support

A factor of both fundamental and practical importance in catalysis, which might change the reaction kinetics on supported systems, is the possibility of adsorption of reactants on the support followed by diffusion to the catalyst particle and vice versa. In the case of CO oxidation, there are experimental reports that the CO supply via the support is important for model nanometer catalysts obtained by evaporating Pd onto mica [18], Al_2O_3 [19], SiO_2 [20] and MgO(100) [21] (see also the reviews [14,22] and recent simulations [13]). In our study [7], this effect was analyzed by treating self-consistently A (CO) adsorption and diffusion on the support and the reaction steps on the catalyst particles. The model used includes catalyst particles regularly distributed on the support. The shape of each identical catalyst particle is of minor importance if we are interested in exploring the role of the support-mediated reactant supply. For this reason, the catalyst particle shape was for simplicity taken to be circular (Fig. 2(a)). The reaction kinetics were in this case calculated by employing the MF approximation (MC simulations of the reaction with reactant diffusion on the support are in principle possible but not necessary).

Typical results obtained in the limit when the A diffusion zones around different catalytic particles are not overlapping (i.e. the particles are sufficiently far

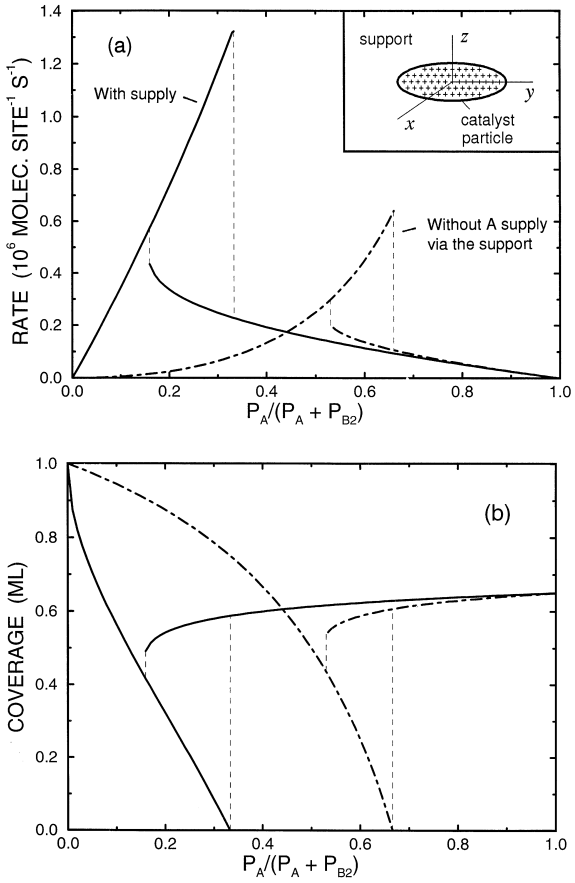

Fig. 2. (a) Reaction rate and (b) reactant coverages for the rapid $2A + B_2 \rightarrow 2AB$ reaction under steady-state conditions. The solid and dashed lines show respectively the kinetics with and without A supply via the support. The results have been obtained for $P_A + P_{B_2} = 0.01$ bar and $T = 450$ K with the kinetics parameters typical for CO oxidation on Pt or Rh (for the details of calculations, see [7]). The insert on panel (a) exhibits the model used in calculations.

apart) are shown in Fig. 2 together with the results corresponding to the case when there is no A supply via the support. Specifically, Fig. 2 exhibits the reaction rate and adsorbate coverages as a function of the reactant pressure ratio, $P_A/(P_A + P_{B_2})$. Due to the A supply from the support, the position of the maximum reaction rate is found to be shifted to a lower value of the reactant pressure ratio. In addition, the dependence of the reaction rate on the reactant pressure (for the regime where P_A is small and the surface is predominantly covered by B) is changed considerably (it becomes almost linear) compared to the case without A diffusion from the support. As $P_A/(P_A + P_{B_2})$ increases from 0 to 1, the system exhibits a transition from a regime where the reaction rate is almost completely controlled by A supply from the support to a regime where diffusion from the support is negligible. Note also that with the action of the support to trap reactant particles, a much higher (in our case by a factor of two) maximum rate becomes possible, compared to the case with an inert support. In addition, the poisoned, low reactive state can be moved to new gas mixing regimes. Experimentally, this type of behaviour can easily be tested by measuring the reaction rate versus gas mixture composition, since the maximum should move in characteristic manner with varying temperature, due to the T-dependence of the effective spillover radius.

2.3. Interplay of kinetics on different facets

During catalytic reactions on nm crystallites, adjacent crystal facets can communicate with each other by reactant diffusion. This effect was simulated [8,9] by assuming that the catalyst particle is shaped into a truncated pyramid (see the inset in Fig. 5), with top and bottom (100) faces and (111) side faces and with the largest (100) facet attached to the substrate. Adsorption of A molecules (step (2)) was considered to occur irreversibly (no desorption) with unit sticking coefficient on all the facets. The B_2 sticking coefficients for the (100) and (111) facets were assumed to be 1 and 0.1, respectively. Diffusion of A molecules on and between facets was considered to be rapid. The reaction kinetics were classified by using the governing parameter, p, defined as the ratio of the A impingement rate to the total impingement rate, i.e. $p = \mathcal{F}_A/(\mathcal{F}_A + \mathcal{F}_{B_2})$.

With increasing p, the model predicts continuous and first-order kinetic phase transitions. The zero-rate regimes at $p < p_1$ and $p > p_2$ (p_1 and p_2 are the critical points) correspond to the surface completely covered by B and A, respectively (complete poisoning is connected with irreversible reactant adsorption and (at p_1) with immobility of B particles). The position of the reaction window where the rate is nonzero depends on the ratio of the A and B_2 sticking coefficients. For the infinite (111) and (100) surfaces, the reaction

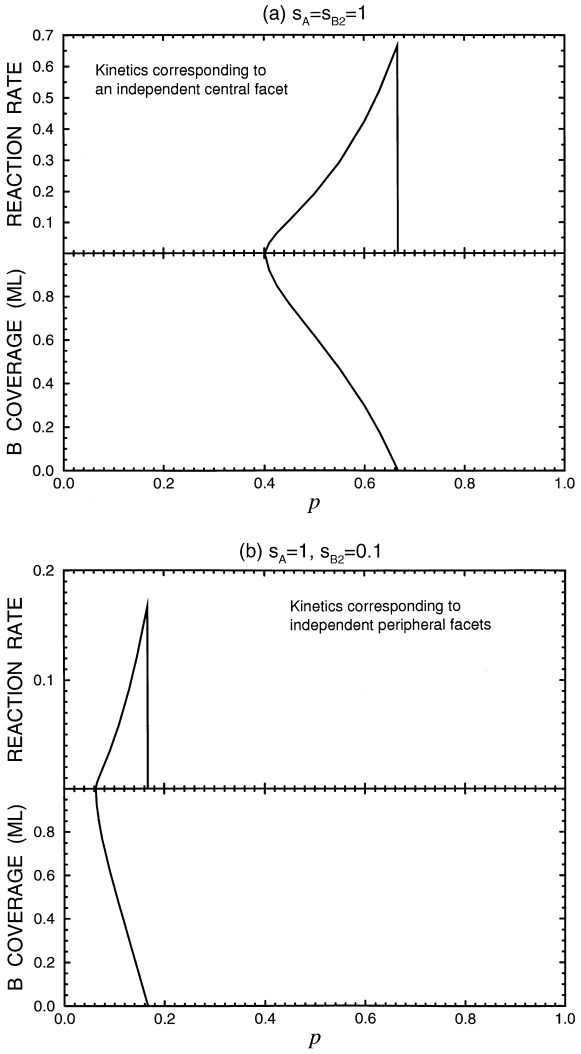

Fig. 3. Reaction rate (A molec. per adsorption attempt) and B coverage for the rapid $2A + B_2 \rightarrow 2AB$ reaction with irreversible A and B_2 adsorption, rapidly-diffusing A particles and immobile B particles. The catalyst surface is infinite. (a) Results for the case when the A and B_2 sticking coefficients are equal, $s_A = s_{B_2} = 1$. (b) As (a) but for $s_A = 1$ and $s_{B_2} = 0.1$. (From [8].)

windows are located (Fig. 3) at relatively low and high values of p, respectively (actually, the kinetics shown in Fig. 3(b) can be converted to that exhibited in Fig. 3(a) by using $\mathcal{F}_A/(\mathcal{F}_A + s_{B_2}\mathcal{F}_{B_2})$ instead of $\mathcal{F}_A/(\mathcal{F}_A + \mathcal{F}_{B_2})$ and properly renormalizing the reaction rate).

If the total reaction rate for a finite catalyst particle were given simply by a superposition of the rates corresponding to two infinite faces, we obtain

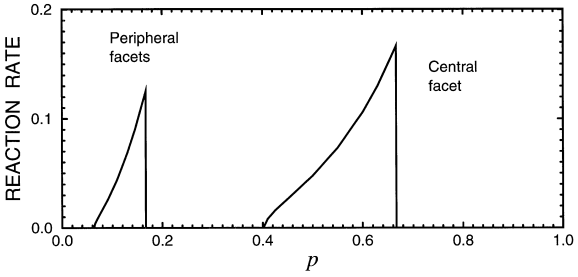

Fig. 4. Rate of the reaction occurring on the nm pyramidal particle with the base size is about 20 nm. The results are obtained by using superposition of the reaction rates shown in Fig. 3(a,b). (From [8].)

the kinetics shown in Fig. 4. However, if there is diffusion-mediated coupling of the reactions on the different facets, we find (Fig. 5) distinctly new kinetics, compared to those for the infinite surfaces, and completely different compared to that predicted by employing the conventional superposition prescription. Specifically, a single new reaction window appears, very different from those on either facet. This can be understood as follows. Compared to the isolated central and peripheral facets, the communicating facets provide new source/drain channels for

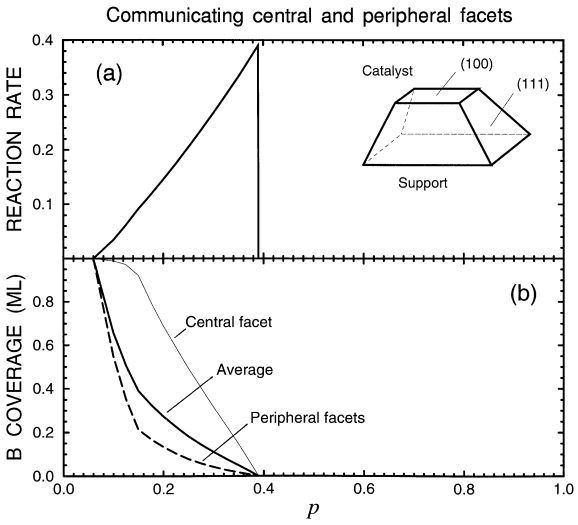

Fig. 5. Reaction rate (A molec. per adsorption attempt) and B coverages for the reaction occurring on the nm pyramidal particle (as shown in the insert) with the basis size of about 20 nm. The thick solid line (on panel (b)) shows the average coverage, the thin solid line corresponds to the coverage of the central facet of the nanoparticle, and the dashed line exhibits the coverage of sites on the peripheral facets. (From [8].)

A particles. The central facet, which in isolation can resist the self-poisoning by *A* particles up to a high value of p, will in the communicating system receive an additional supply of *A* particles from the adjacent peripheral area, which is less resistant to *A* poisoning since the B_2 sticking coefficient is much smaller there. This latter net flow of *A* particles from the peripheral to the central area facilitates *A* poisoning of the central facet at high values of p and simultaneously prevents *A* poisoning from occurring on the peripheral area at relatively low values of p.

The results shown in Figs. 3–5 were obtained [8] in the limit when *A* diffusion is much faster compared to the LH step. In a later extension of this work [9], the rate of *A* diffusion was varied systematically from low to high values.

2.4. Adsorbate-induced reshaping of crystallites

Crystallite shape transformations, due to adsorbed reactants, may affect the steady-state kinetics of catalytic reactions. In particular, adsorbates can change the surface energy situation of a crystallite participating in a catalytic reaction, so that it transforms into a new shape with new kinetic conditions. To study such transformations, we combined MC simulations of the $A + B_2$ reaction kinetics with the use of the Wulff rule to find the optimum crystallite shape [10]. In the absence of adsorbates, the equilibrium particle shape was assumed to be a truncated pyramid with the (111) and (100) facets. During reaction, the particle shape and reaction kinetics were calculated self-consistently by assuming a linear dependence of the surface tension of the (100) facet on *B* coverage (shape transformations were considered to occur instantaneously when they were energetically favourable). If this dependence is sufficiently strong, the pyramid-shaped catalyst particles become unstable with respect to reconfiguration to the parallelepiped shape with (100) facets. Such reconfiguration results in shifting the reaction window to higher values of p (Fig. 6).

The effect described is of generic nature. At present, there is no guarantee that it really takes place in CO oxidation on Pt, Rh, or Pd crystallites (although the experiment [23] indicates that oxygen adsorption on Pd crystallites does stabilize the (100) facets). It might however occur in other reactions. For example, the

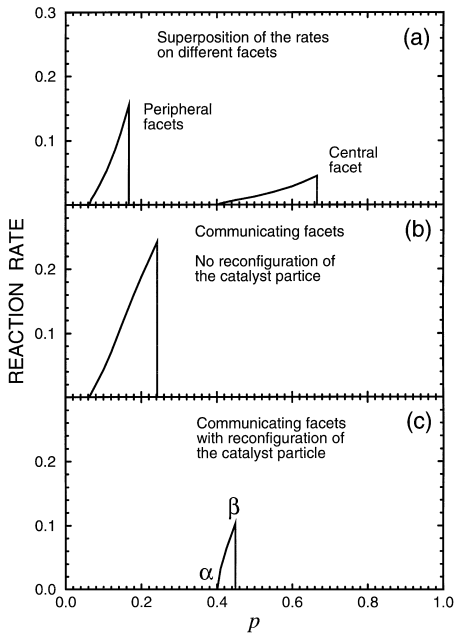

Fig. 6. Reaction rate (*A* molec. per adsorption attempt) of the $A + B_2$ reaction on a supported catalyst as a function of the ratio of the *A* impingement rate to the total impingement rate. The B_2 sticking coefficients for adsorption on the (111) and (001) facets are 0.1 and 1, respectively. The *A* sticking coefficient is equal to unity for both facets. Panel (a) shows superposition of the reaction rates on independent facets. Panel (b) demonstrates the reaction kinetics for the crystallite with communicating facets and fixed particle shape and facet areas (the relative surface areas correspond to the clean pyramid crystallite). Panel (c) exhibits the corresponding kinetics when a change in particle shape from truncated pyramid to parallelepiped is allowed. Along the line $\alpha\beta$, the catalyst is shaped as a parallelepiped. The point β corresponds to reconfigurating the catalyst shape from a parallelepiped to a pyramid. (From [10].)

TEM study [24] shows that heating of the model supported Pt catalyst at 500°C in a mixture of hydrogen sulphide and hydrogen results in reshaping of the Pt particles from rounded to approximately cubic shapes, indicative of (100) faceting.

If the adsorbate-induced transition from one shape to another is energetically impossible, the adsorbate-induced changes in the relative areas of different facet may still take place and influence the reaction kinetics. An interesting example illustrating this case has recently been given by Ovesen et al. [25]. They have analyzed the kinetics of methanol

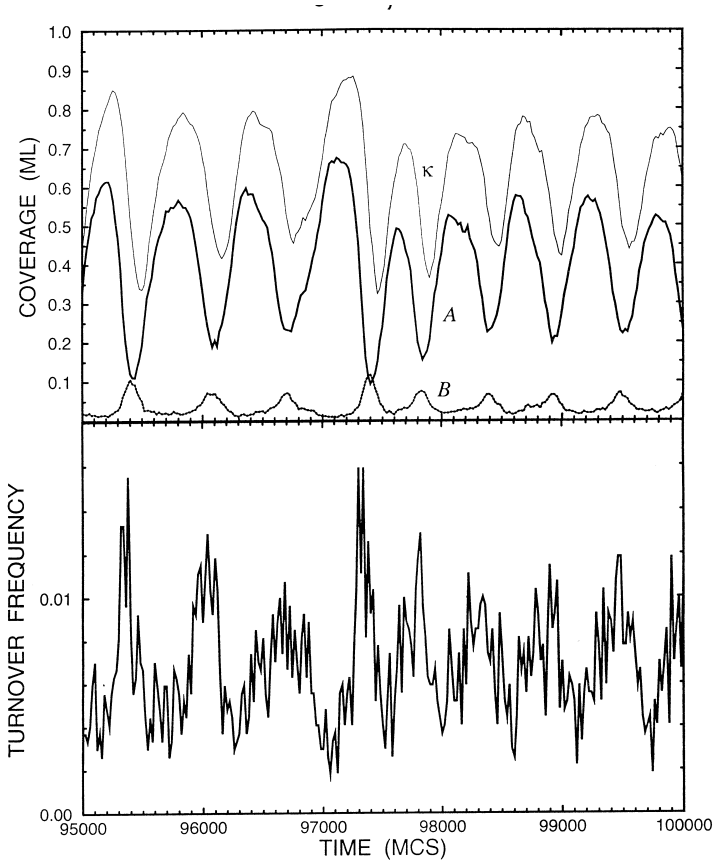

Fig. 7. A and B coverages, fraction of surface sites in the restructured state, κ, and reaction rate (AB molec. site^{-1} MCS^{-1}) as a function of time for the $A + B_2$ reaction on the separate central facet. (From [11].)

synthesis on nm Cu particles supported by ZnO. The generalized surface tension for the substrate-particle interface was assumed to be dependent on the reduction potential of the gas phase. The latter resulted in the dependence of the areas of the (111), (100) and (110) facets on the gas-phase concentrations (such changes were observed by using EXAFS). The total reaction rate, represented as a sum of the reaction rates on different facets, was found to be strongly affected by the changes in particle morphology.

2.5. Oscillations and chaos

Kinetic oscillations in reactions on single-crystal surfaces are often connected with adsorbate-induced surface restructuring [3,26]. We have recently demonstrated [11] that on the mesoscopic scale such oscillations may exhibit unique features due to diffusion communication between facets. The model employed was similar to that described in Section 2.3. The new key factor was that the central (100) facet was allowed to reconstruct during A adsorption, as in the case of CO adsorption on the Pt(100) single-crystal surface. This phenomenon was treated as a first-order phase transition by using a well-defined lattice-gas model [27].

First, we calculated (Figs. 7 and 8) the reaction kinetics for the separate central 50×50 facet. In this case, the amplitude of oscillations is high. The large-scale changes in adsorbate coverages are accompanied by small-scale fluctuations with the amplitude

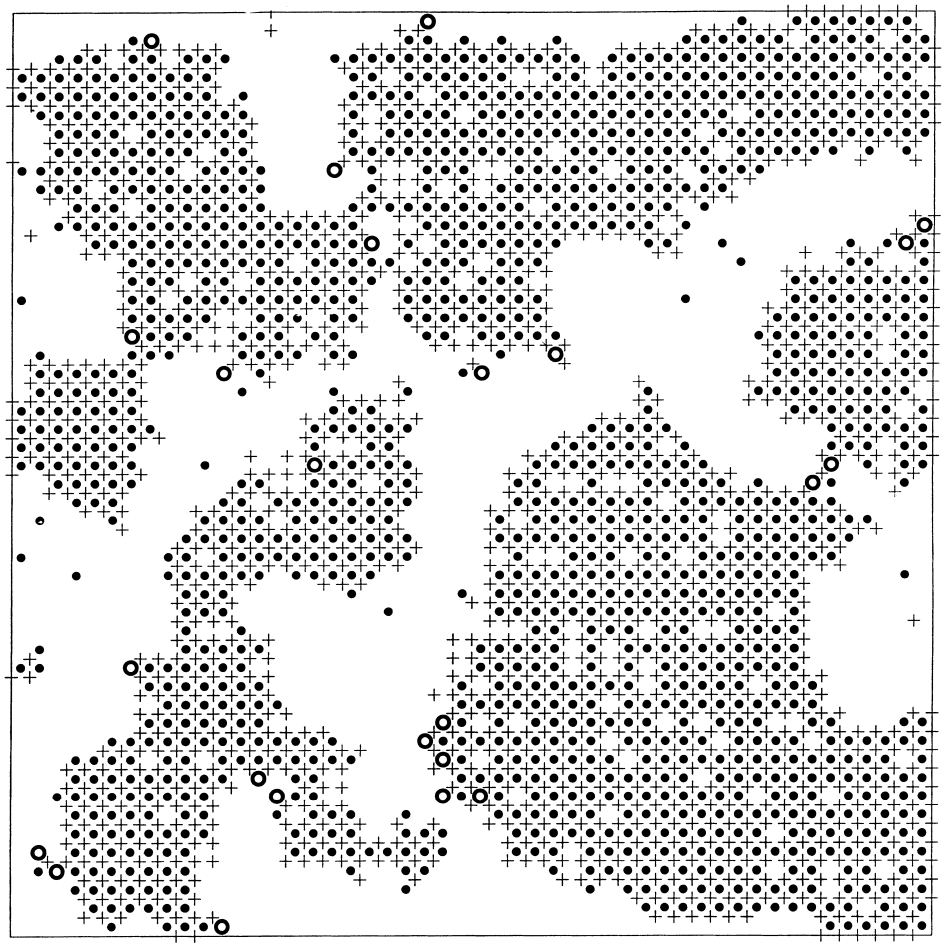

Fig. 8. Typical snapshot of the central facet during the MC run shown in Fig. 7. Pluses correspond to surface sites in the restructured state (the unrestructured sites are not shown). Filled and open circles exhibit *A* and *B* particles. (From [11].)

comparable with that predicted by the Poisson distribution. The fluctuations in the reaction rate are larger, because the rate depends on the distribution of both reactants.

In the case of communicating facets, the main role of the peripheral facets is to provide additional supply of *A* particles to the central facet via adsorption and surface diffusion. This supply results (Figs. 9 and 10) in a strongly nonuniform phase distribution on the central facet (the facet is restructured primarily near the boundaries). As a consequence, the conditions for oscillations on different regions of the central facet are quite different. In other words, the system possesses a wide distribution of oscillation frequencies (in addition the kinetics become very sensitive with respect to small fluctuations in adsorbate coverages). The important point is that different regions are strongly interconnected via adsorbate diffusion. These special features taken as a whole result in chaotic oscillations (Fig. 9). Such chaos, connected with the interplay of the reaction kinetics on adjacent (100) and (111) facets, seems to be inherent for reactions on nm particles or on a tip of a field ion microscope [28] and can hardly be observed in reactions on single-crystal surfaces. An interesting question not addressed here is when such oscillations and chaos are phase-coupled or totally uncoupled, respectively, for particle arrays.

3. Role of edges

Our recent results reviewed above were obtained assuming that the reaction occurs primarily on the facets of a catalyst particles. The properties of edge and facet sites were considered to be similar. In reality, the edge sites might be catalytically more (or less) active compared to the facet sites. The difference between these sites is expected to be qualitatively similar to the difference between the facet and step sites on single-crystal surfaces. Bearing in mind this analogy, it is appropriate to recall some key experimental findings [4] concerning the role of steps in CO oxidation on Pt. First, it is worth to note that oxygen and CO prefer to adsorb on steps. The binding energy on steps is slightly higher than on terraces both for oxygen and CO. The O_2 sticking coefficient is often reported to be higher on steps than on terraces. In addition, oxygen on step sites can be more reactive than on the terrace sites. On the Pt(335) surface (this surface contains narrow (111) terraces), for example, the CO_2 TPR peaks have been found [4] to occur at $T \approx 250\,\mathrm{K}$. At similar conditions on the Pt(111) face, CO_2 is formed at $T \approx 325\,\mathrm{K}$ [29]. Using the standard Redhead equations with the 'normal' pre-exponential factor ($\nu_{\mathrm{LH}} \simeq 10^{12}$–$10^{13}\,\mathrm{s}^{-1}$ [30]), one can easily estimate from these data that the activation energy for the LH step is, respectively, 16 and 21 kcal/mol in these cases. This means, e.g., that at $T = 400\,\mathrm{K}$ the reaction on step sites might be about 500 times faster than on terrace sites.

In this section, we present MC simulations illustrating the effect of edges on the kinetics of the $A + B_2$ reaction (steps (2)–(4)) occurring on a nm catalyst particle. The results presented are new. For this reason, we describe the model, algorithm of simulations and obtained results in more detail than in Section 2.

3.1. Model

Our model system is a supported particle (Fig. 11(a)) with two types of surface facets, (111) and (001). The bottom facet is assumed to be attached to the support. The active surface of the particle is modeled (Fig. 11(b)) as a two-dimensional 100×100 lattice, where the central 50×50 part mimics the top (001) facet, and the periphery represents the four (111) side facets. For simplicity, the arrangement of adsorption sites on both parts of the lattice is considered to have square symmetry (on the (111) facets, the adsorption sites are of course not four-coordinated, but the latter is usually of minor importance compared to the facet-related difference in the kinetic parameters of elementary reaction steps). Adsorption sites at edges, between the (111) and (001) facets, are assumed to be located symmetrically on both sides of the border between the facets (one site on each side along the border). Thus, the edges are mimicked by two rows of sites located on the boundaries between the central and peripheral parts of the lattice. The properties of these edge sites are assumed to be different compared to those of the terrace sites. Specifically, we treat below three cases when (i) the B_2 adsorption occurs on edge sites with a higher sticking probability than on the facets, (ii) the reactivity on the edge sites is higher than on the facets (i.e. the activation energy is lower), and (iii) the A binding energy on the edge sites is higher than on the facets.

In addition to the edge sites between the (111) and (100) facets, the truncated pyramid (Fig. 11(a)) has

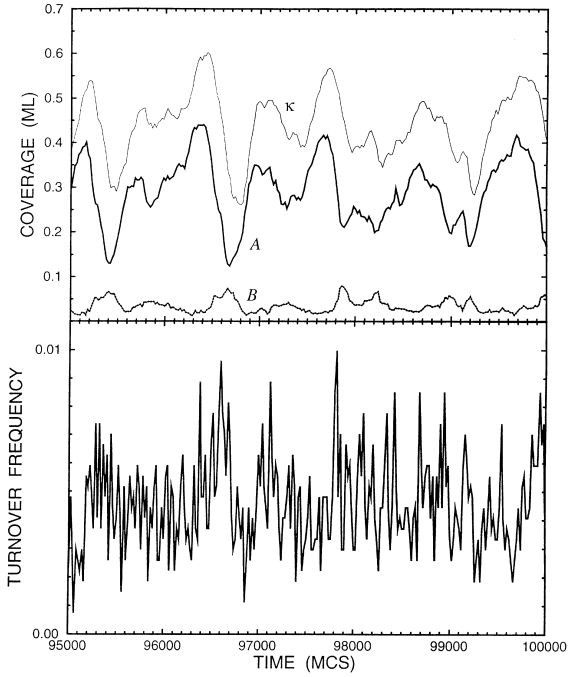

Fig. 9. Chaotic reaction kinetics for the nm particle with communicating facets. (From [11].)

edge sites between the (111) facets. The properties of these sites might also be different compared to those of the (111) and (100) facets. In the present analysis, the latter is ignored for simplicity and transparency.

3.2. Algorithm of simulations

In many real systems (e.g. in CO oxidation on Pt [7]), A diffusion is much faster compared to the LH step, which in turn is faster than (or comparable with) B diffusion. This situation can be described by using a specially designed MC algorithm [8], which is explicitly based on the high difference in the rates of adsorption, reaction and diffusion. In the present study, we use a more general MC algorithm allowing us to include finite and widely different rates of different reaction steps. The algorithm is also suited for including special features of, e.g., the edge sites, affecting the reaction kinetics.

As in Section 2, the main governing parameter is the ratio of the A impingement rate to the total impingement rate, $p = \mathcal{F}_A/(\mathcal{F}_A + \mathcal{F}_{B_2})$. With this choice, it is convenient to normalize the rates of all the steps to the total impingement rate. In this case, the A and B_2 adsorption rates are simply p and $(1 - p)$ times the corresponding sticking coefficient. To transform the rate of n different processes into probabilities, we generate the probability limits, P_i, through the ratios

$$P_i = \frac{\sum_{j'=1}^{i} k_{j'}}{\sum_{j=1}^{n} k_j}$$

where k_j denotes the rate constant of process j. If the rate constants for a given process (e.g. for B_2 adsorption) are different on different parts of the lattice, we choose the maximum rate constant. Thus, we generate a normalized probability room between zero and one, where the length of the probability interval is proportional to the magnitude of the different rates. For instance, the probability length for process 1 is P_1, the probability length for process 2 is $(P_2 - P_1)$, etc. To simulate the time evolution in the system, we select a site at random. Then, a random number between zero and one is chosen. If the number is between zero and P_1, process 1 is tried. If the number is between P_1 and P_2, process 2 is tried, etc. However, if the event actually occurs or not depends on the nature of the process (adsorption, diffusion, or reaction) as described below.

1. Adsorption of A occurs irreversibly if the chosen site is vacant. The sticking coefficient for A adsorption is assumed to be unity for all the sites.
2. For dissociative adsorption of B_2, we choose two nearest-neighbour sites at random, which have to be vacant in order to result in a possible adsorption event. If the latter is the case, the different sticking coefficients on different parts of the lattice have to be taken into account (practically, this means that the adsorption probability is given by the ratio of the sticking coefficient for a given pair of sites and the maximum B_2 sticking coefficient).
3. For A diffusion, we select at random a nearest-neighbour site which has to be vacant in order to obtain a successful diffusion event. Then, the process is realized with the probability, $k_{dif}^{A}/k_{dif}^{max}$, where k_{dif}^{A} is the jump rate constant for an A particle located in a given site, and k_{dif}^{max} is the maximum jump rate constant.
4. B diffusion is treated in analogy with A diffusion.
5. For the $A + B \rightarrow AB$ step, followed by AB desorption, the chosen site should be occupied by A or B. If this is the case, we choose randomly a nearest-neighbour site which also has to be occupied by a particle of the opposite kind compared to its neighbour. If this happens, the reaction occurs, i.e., the selected AB pair is removed from the lattice with the probability k_r/k_r^{max}, where k_r is the reaction rate constant for this pair, and k_r^{max} is the maximum reaction rate. The residence time of AB particles on the surface is assumed to be negligible.

All the results presented below were obtained by initially executing $100 \times L \times L$ attempts of B_2 adsorption ($L = 100$ is the lattice size), which gives a B coverage of the lattice close to 0.91. The number of MC steps used to get the steady-state kinetics was typically 10^6 (1 MC step corresponds to $L \times L$ attempts to realize one of the processes). To determine whether the steady-state was reached for a given gas-mixture ratio, convergence criteria for the sum of the variations in the A coverage, B coverage and reaction rate were imposed. Simulation runs were terminated if the sum of the mean-values of 10^5 MC steps had a variation smaller than 10^{-3}.

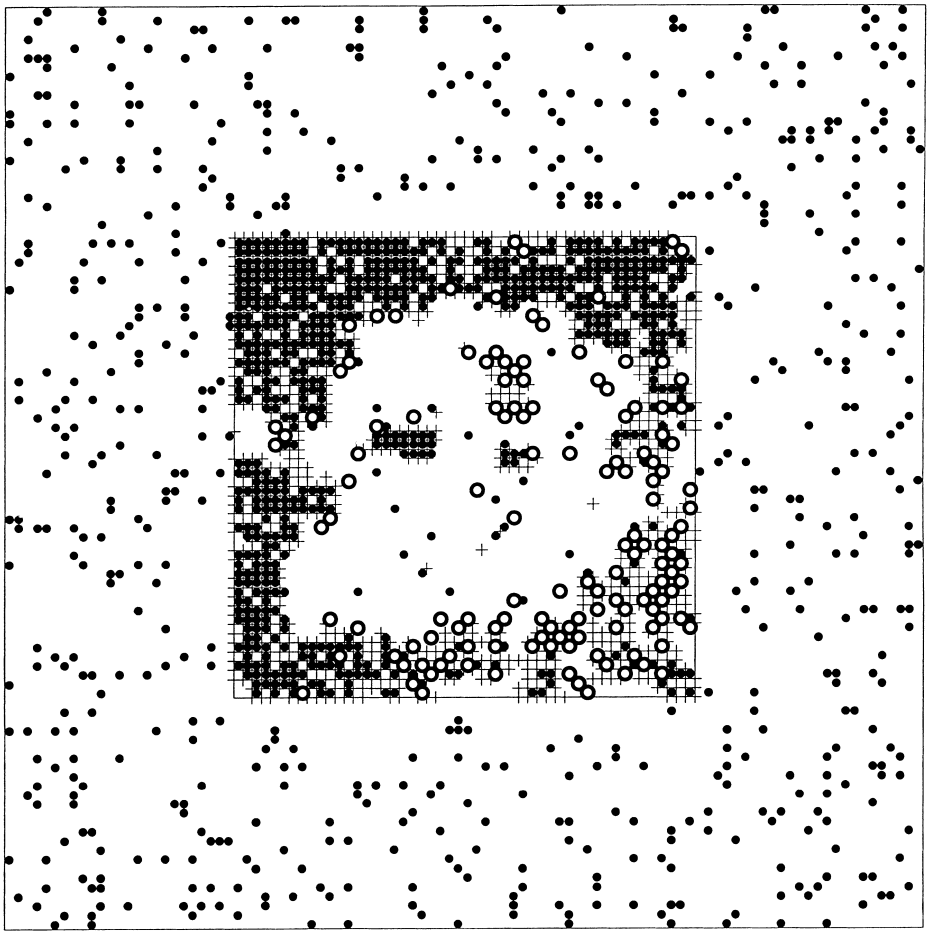

Fig. 10. Typical snapshot of the central and peripheral facets during the MC run shown in Fig. 9. The designations are as in Fig. 8. (From [11].)

3.3. Results of simulations

In our simulations, *A* (CO) diffusion is assumed to be faster than the LH step, which in turn is faster than *B* (O) diffusion. Elementary estimations show that these conditions are realized if the former two steps occur on the facets with the rate constants $k_{\mathrm{dif}}^{\mathrm{A}} = 10\,000$ and $k_{\mathrm{r}} = 500$ (one of course may use larger values of these rate constants but practically it is not necessary). The B_2 adsorption is assumed to occur with different sticking probabilities on the central and peripheral facets and also on the edges. For the facets, the B_2 sticking probabilities are chosen to be $s_{\mathrm{B_2}}^{\mathrm{c}} = 0.1$ and $s_{\mathrm{B_2}}^{\mathrm{p}} = 0.05$ (c=centre, p=peripheral). As a *reference case*, we calculated the reaction kinetics (Fig. 12) by considering that the kinetic properties of the edge sites are the same as those of the central facet. Then, the kinetic parameters characterizing the reaction steps on the edges were successively varied.

The first of the latter examples is to allow the B_2 sticking coefficient on the edges to be higher than on the facets. Specifically, we use $s_{\mathrm{B_2}}^{\mathrm{e}} = 1$ (we call this the '*standard*' case in the later comparisons). The increase of $s_{\mathrm{B_2}}^{\mathrm{e}}$ from 0.1 to 1 is found (Fig. 12) to result in a large shift of the right end of the overall reaction window (where the *A* poisoning occurs) to a much higher *p*-value, while the reaction rate for

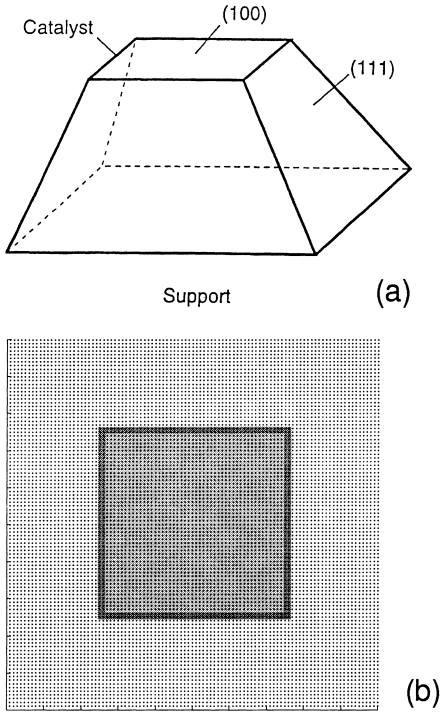

Fig. 11. (a) Pyramidal supported metal particle and (b) its 2D analogue (a 100 × 100 lattice) used in simulations. The central sites (panel (b)) are displayed with a light grey background while the peripheral sites have a white background. The edge sites are shown with a dark grey background.

lower p-values are unaffected. This widening of the reaction window occurs because the higher B_2 sticking coefficient on the edges increases the supply of B_2 molecules and thus shifts the A poisoning transition to higher p-values. At low p-values, the reaction is deficient in A and not affected by the increased B supply.

Typical snapshots of the lattice for the reference and standard cases are shown in Figs. 13 and 14, respectively. For $p = 0.05$, the distributions of B particles on the lattice are quite similar in the two cases (Fig. 13(a) and Fig. 14(a)). At $p = 0.10$, the B coverage on the central facet is higher than in the standard case (Fig. 13(b) and Fig. 14(b)). For $p = 0.15$, the lattice is completely poisoned by A in the reference case, while the standard case shows a highly reactive state (Figs. 13(c) and Fig. 14(c)). Thus, even though the number of edge sites is limited (4% of the total number of sites), they change the reaction kinetics dramatically, solely through a higher B_2 sticking coefficient.

The next case we consider is when the *reactivity on the edge sites* is higher than on the other parts of the surface. Keeping the bulk of the parameters the same as in the standard case, we have increased the reaction rate constant for the edge sites from 500 up to 2500. The effect of this change on the reaction rate is found to be nearly negligible (Fig. 15). Actually, the changes in the reaction rate are fairly minor even if we increase the reaction rate over the whole lattice. The reason is that the reaction is primarily controlled by adsorption. To obtain noticeable changes in the reaction window by varying the reaction rate constant on the edges, the reaction rate constants on the edges and the rest of the surface should be substantially different and in addition one of them is required to be comparable in magnitude to the adsorption rate constants.

The lattice snapshots corresponding to the case (Fig. 15) when the reactivity of the edge sites is higher than on the facet sites are shown in Fig. 16 for $p = 0.05$, 0.10 and 0.15. Compared to the standard case, a clear difference is seen for $p = 0.15$ (cf. Fig. 14(c) and Fig. 16(c)). In particular, the A particles adsorb primarily on the peripheral part of the lattice and then diffuse to the central part in order to react with B

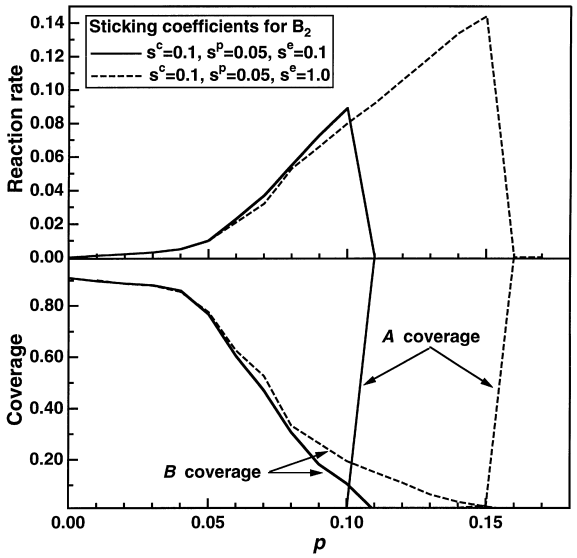

Fig. 12. Rate of AB production (per one adsorption attempt) and average reactant coverage for $k_r = 500$, $k_{dif}^A = 10\,000$, $k_{dif}^B = 0$, $s_{B_2}^p = 0.05$, and $s_{B_2}^c = 0.1$. The two sets of the data correspond to $s_{B_2}^e = 0.1$ (the reference case) and $s_{B_2}^e = 1$ (the standard case), respectively.

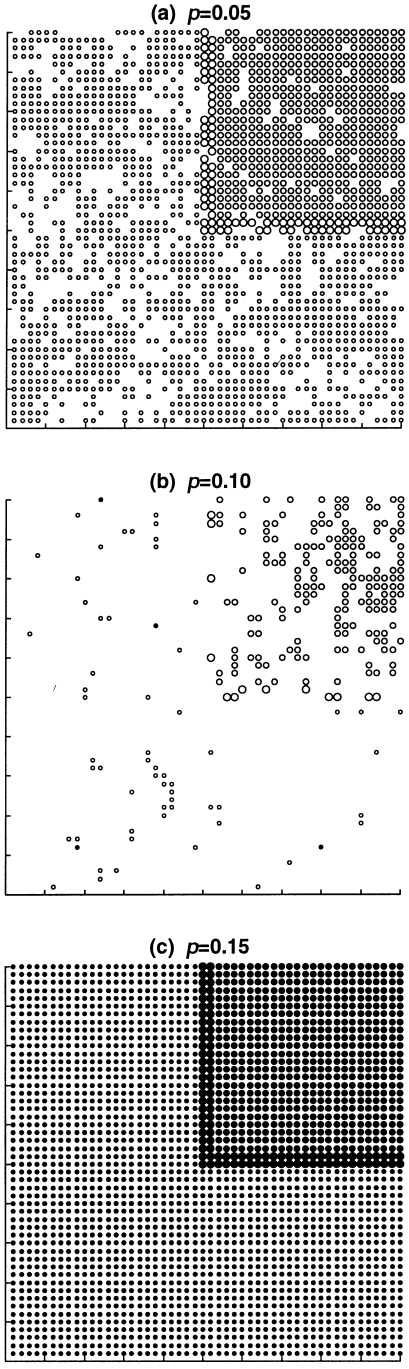

Fig. 13. Snapshots of the lower left quadrant of the lattice at steady state for the reference case (Fig. 12) at $p = 0.05$ (a), 0.10 (b) and 0.15 (c). Filled and open circles denote *A* particles and *B* particles, respectively. The size of the circles (small, medium or large) indicate location of the particles on the lattice (the peripheral, central or edge part).

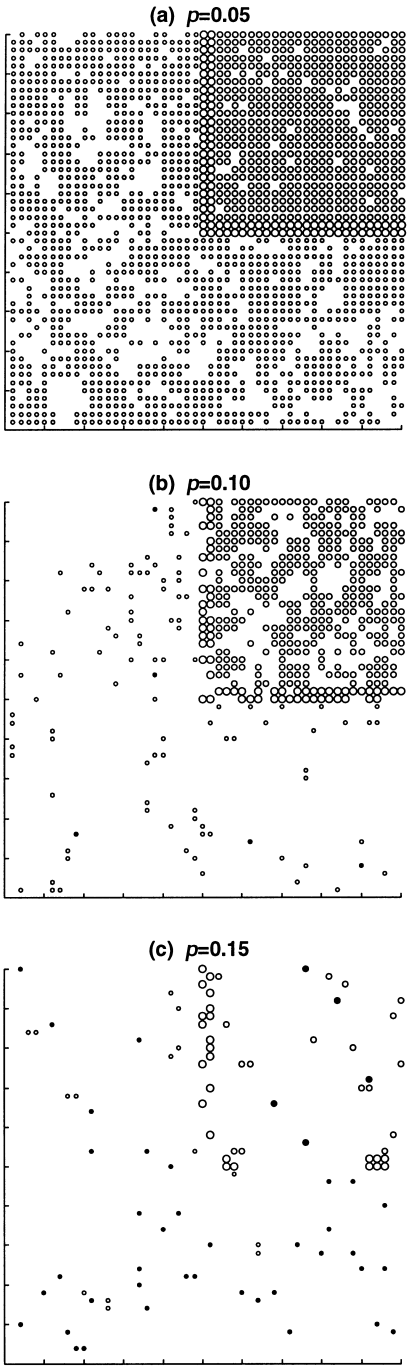

Fig. 14. As in Fig. 13, but for the standard case.

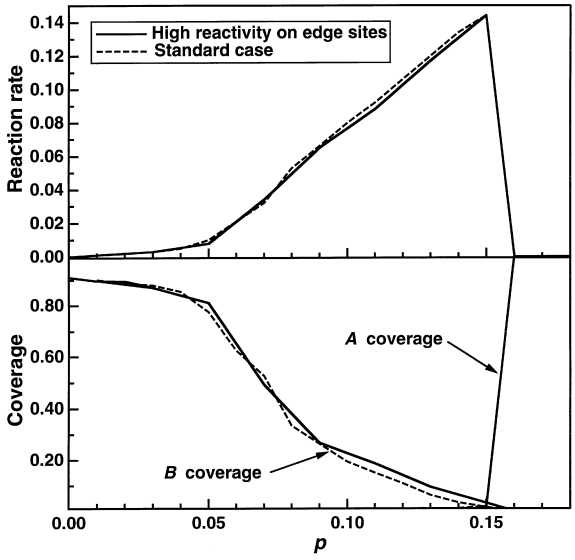

Fig. 15. Reaction rate and average reactant coverages as a function of p for the standard case and for the case of high reactivity on edge sites ($k_r^e = 2500$).

particles. To reach the central part, they should pass the edge sites. With increasing reactivity of the edge sites (from 500 up to 2500), a larger number of A particles react on the edges and thus the higher B coverage is maintained on the central part. These local variations in the distribution of B particles do not however affect the integral reaction rate.

The third effect studied is related to the A binding energy on the edge sites. If A adsorption on these sites is energetically favourable, the rate of A jumps from the edges to the facets will be lower compared to that for jumps on the facets. In our simulations, the rate constant for jumping out from edge sites to either the central or peripheral parts of the lattice was reduced from the standard value $k_{dif}^{A} = 10\,000$ down to 1000 (all the other parameters were kept as in the standard case). The resulting changes in the reaction kinetics are found (Fig. 17) to be minor, because the A diffusion step is still much faster than the rate-limiting adsorption steps. Typical snapshots of the lattice in the case under consideration are shown in Fig. 18 for $p = 0.05$, 0.10 and 0.15. Compared to the standard case, a clear effect of the suppression of A diffusion from the edges is again seen at $p = 0.15$ (cf. Fig. 14(c) and Fig. 18(c)). As in the case of the high reactivity of edge sites (Fig. 16(c)), the coverage of the central

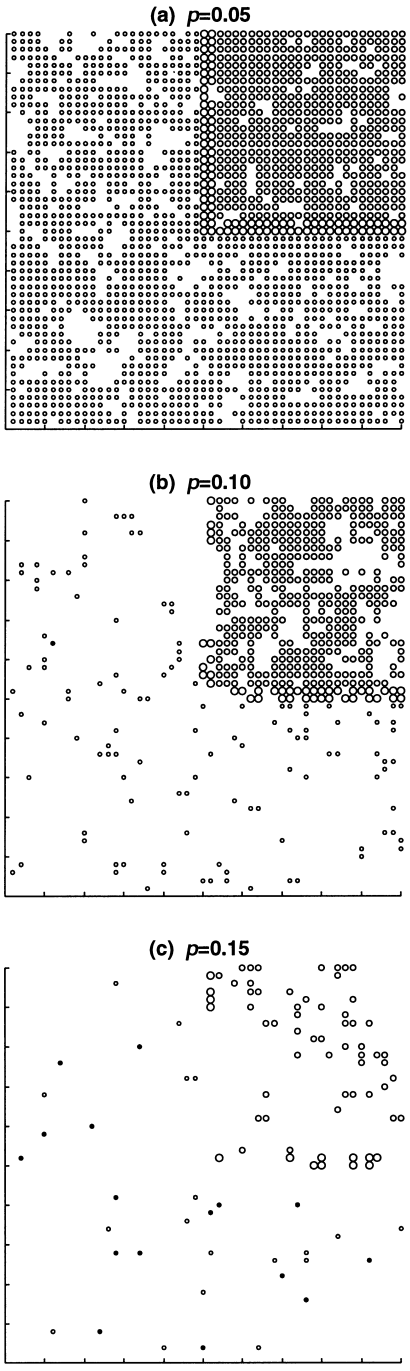

Fig. 16. Snapshots of the lower left quadrant of the lattice for the case of high reactivity on edge sites (Fig. 15) at $p = 0.05$ (a), 0.10 (b) and 0.15 (c). The designations are as in Fig. 13.

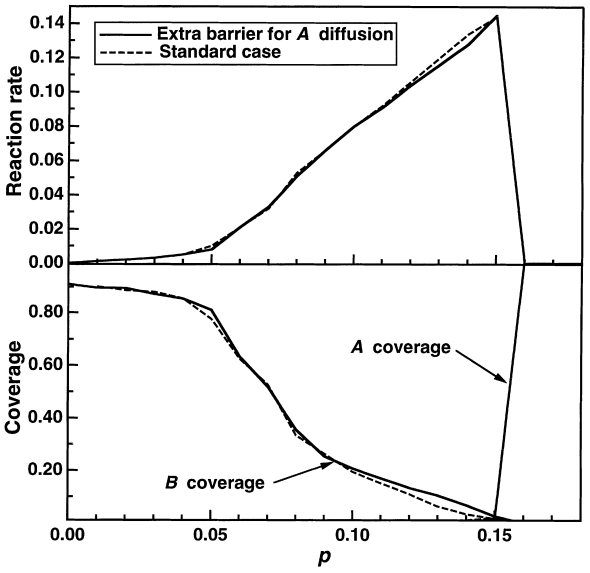

Fig. 17. Reaction rate and average reactant coverages as a function of p for the standard case and for the case of a higher barrier for diffusion from the edge sites to the facet sites ($k_{\mathrm{dif}}^{\mathrm{A}} = 1000$).

facet by B particles becomes larger. Thus, there can be local variations in the surface coverage due to an extra high diffusion barrier on the edge sites, but the overall reaction rate remains relatively unaffected by such variations, for the studied parameter range.

In summary, we have shown that in the case of rapid catalytic reactions the effect of the edge sites on the reaction rate can be considerable if the sticking coefficient for these sites is higher than for facets. With regard to the diffusion and reaction steps, they have to be slowed down towards that of the (rate-limiting) adsorption step to cause significant effects in the global kinetics.

4. Conclusion

The results presented above show explicitly that the kinetics of catalytic reactions occurring on nm-sized metal particles, exposing different crystalline facets, can be dramatically different from the mere superposition of the kinetics of the individual facets. This has been – qualitatively – realized for a long time and attributed to a number of different effects. However, the fact that purely kinetic factors such as inter-facet diffusion create unique new kinetics has not been quan-

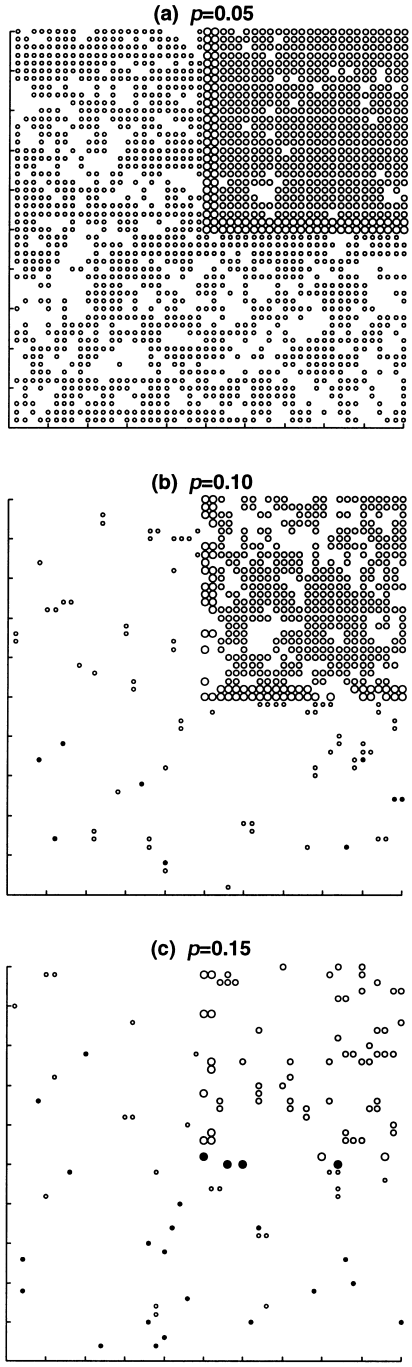

Fig. 18. Snapshots of the lower left quadrant of the lattice in the case of a higher barrier for diffusion from the edge sites to the facet sites (Fig. 17) at $p = 0.05$ (a), 0.10 (b) and 0.15 (c). The designations are as in Fig. 13.

tified. The conceptual base, provided by the present simulations of catalytic kinetics on the nm scale, will help designing and interpreting new experiments that systematically address the so-called structure and pressure gaps in catalysis. A prerequisite for such studies is the combination of well defined and characterized model systems of catalyst particle arrays [6,14,15] and accompanied simulations. The most important kinetic measurements will be the rate versus gas-composition curves, at appropriate choices of absolute pressure and temperature, for well studied model systems such as $CO+O_2$, CO+NO, H_2+O_2 on the noble metals.

Acknowledgements

This work has been supported by the Swedish Engineering Research Council and the Competence Centre for Catalysis, which is funded by the Swedish National Energy Administration and the member companies including AB Volvo, Johnson Matthey CSD, Saab Automobile AB, Perstorp AB and MTC AB. One of us (V.P. Zh.) is grateful for the Waernska Guest Professorship at Göteborg University.

References

[1] J.M. Thomas, W.J. Thomas, Principles and Practice of Heterogeneous Catalyst, VCH, Weinheim, 1997.
[2] M. Shelef, G.W. Graham, Catal. Rev. Sci. Eng. 36 (1994) 433.
[3] R. Imbihl, G. Ertl, Chem. Rev. 95 (1995) 697.
[4] J.T. Yates, J. Vac. Sci. Technol. A 13 (1995) 1359.
[5] M. Che, C.O. Bennett, Adv. Catal. 36 (1989) 55.
[6] P.L.J. Gunter, J.W. Niemantsverdriet, F.H. Ribeiro, G.A. Somorjai, Catal. Rev. Sci. Eng. 39 (1997) 77.
[7] V.P. Zhdanov, B. Kasemo, J. Catal. 170 (1997) 377.
[8] V.P. Zhdanov, B. Kasemo, Surf. Sci. 405 (1998) 27.
[9] H. Persson, P. Thormählen, V.P. Zhdanov, B. Kasemo, J. Vac. Sci. Techn. A 17(4) (1999) 1721.
[10] V.P. Zhdanov, B. Kasemo, Phys. Rev. Lett. 81 (1998) 2482.
[11] V.P. Zhdanov, B. Kasemo, Surf. Sci. Rep., in press.
[12] A.S. McLeod, L.F. Gladden, J. Catal. 173 (1998) 43.
[13] A.S. McLeod, Catal. Today (this issue).
[14] C.R. Henry, Surf. Sci. Rep. 31 (1998) 231.
[15] K. Wong, S. Johansson, B. Kasemo, Faraday Disc. 105 (1997) 237.
[16] V.P. Zhdanov, B. Kasemo, Surf. Sci. Rep. 20 (1994) 111.
[17] E.V. Albano, Heter. Chem. Rev. 3 (1996) 389.
[18] V. Matolin, E. Gillet, Surf. Sci. 166 (1986) L115.
[19] F. Rumpf, H. Poppa, M. Boudart, Langmuir 4 (1988) 722.
[20] M. Eriksson, L.-G. Petersson, Surf. Sci. 311 (1994) 139.
[21] C. Becker, C.R. Henry, Surf. Sci. 352 (1996) 457.
[22] I. Stara, V. Matolin, Surf. Sci. Lett. 4 (1997) 1353.
[23] H. Graoui, S. Giorgio, C.R. Henry, Surf. Sci. 417 (1998) 350.
[24] P.J.F. Harris, Intern. Mater. Rev. 40 (1995) 97.
[25] C.V. Ovesen, B.S. Clausen, J. Schiotz, P. Stoltze, H. Topsoe, J.K. Norskov, J. Catal. 168 (1997) 133.
[26] M. Gruyters, D.A. King, J. Chem. Soc. Faraday Trans. 93 (1997) 2947.
[27] V.P. Zhdanov, B. Kasemo, J. Stat. Phys. 90 (1998) 79.
[28] V. Gorodetskii, J. Lauterbach, H.H. Rotermund, J.H. Block, G. Ertl, Nature 370 (1994) 276.
[29] A. Sabo, M. Kiskinova, J.T. Yates, J. Chem. Phys. 90 (1989) 4604.
[30] V.P. Zhdanov, Elementary Physicochemical Processes on Solid Surfaces, Plenum Press, New York, 1991.